International Journal of Radiation Oncology biology • physics

www.redjournal.org

Physics Contribution

Quantitative Characterization of Tumor Proximity to Stem Cell Niches: Implications on Recurrence and Survival in GBM Patients

Yi Lao, PhD,* Victoria Yu, PhD,† Anthony Pham, MD,‡ Theodore Wang, PhD,‡ Jing Cui, PhD,‡ Audrey Gallogly, PhD,‡ Eric Chang, MD,‡ Zhaoyang Fan, PhD,§ Tania Kaprealian, MD,* Wensha Yang, PhD,‡ and Ke Sheng, PhD*

**Department of Radiation Oncology, University of California - Los Angeles, California; †Department of Medical Physics, Memorial Sloan Kettering Cancer Center, New York, New York; ‡Department of Radiation Oncology, University of Southern California, Los Angeles, California; and §Department of Radiology, University of Southern California, Los Angeles, California*

Received Sep 26, 2020. Accepted for publication Feb 8, 2021.

Purpose: Emerging evidence has linked glioblastoma multiforme (GBM) recurrence and survival to stem cell niches (SCNs). However, the traditional tumor−ventricle distance is insufficiently powered for an accurate prediction. We aimed to use a novel inverse distance map for improved prediction.

Methods and Materials: Two T1-magnetic resonance imaging data sets were included for a total of 237 preoperative scans for prognostic stratification and 55 follow-up scans for recurrent pattern identification. SCN, including the subventricular zone (SVZ) and subgranular zone (SGZ), were manually defined on a standard template. A proximity map was generated using the summed inverse distances to all SCN voxels. The mean and maximum proximity scores (PS_{m-SCN} and $PS_{max-SCN}$) were calculated for each primary/recurrent tumor, deformably transformed into the template. The prognostic capacity of proximity score (PS)-derived metrics was assessed using Cox regression and log-rank tests. To evaluate the impact of SCNs on recurrence patterns, we performed group comparisons of PS-derived metrics between the primary and recurrent tumors. For comparison, the same analyses were conducted on PS derived from SVZ alone and traditional edge/center-to-ventricle metrics.

Results: Among all SCN-derived features, PS_{m-SCN} was the strongest survival predictor ($P < .0001$). $PS_{max-SCN}$ was the best in risk stratification, using either evenly sorted ($P = .0001$) or k-means clustering methods ($P = .0045$). PS metrics based on SVZ only also correlated with overall survival and risk stratification, but to a lesser degree of significance. In contrast, edge/center-to-ventricle metrics showed weak to no prediction capacities in either task. Moreover, PS_{m-SCN}, PS_{m-SVZ}, and center-to-ventricle metrics revealed a significantly closer SCN distribution of recurrence than primary tumors.

Conclusions: We introduced a novel inverse distance-based metric to comprehensively capture the anatomic relationship between GBM tumors and SCN zones. The derived metrics outperformed traditional edge or center distance-based

Corresponding authors: Ke Sheng, PhD, Wensha Yang, PhD; E-mail: Wensha.Yang@med.usc.edu or ksheng@mednet.ucla.edu

Wensha Yang and Ke Sheng made equal contributions to this study.

Disclosures: None.

Research data are stored in an institutional repository and will be shared upon request to the corresponding author.

Acknowledgments—The work presented is supported in part by AAPM Research Seed Grant, NIH R01CA188300, and NIH EB029088.

Int J Radiation Oncol Biol Phys, Vol. 110, No. 4, pp. 1180−1188, 2021
0360-3016/$ - see front matter
https://doi.org/10.1016/j.ijrobp.2021.02.020

measurements in overall survival prediction, risk stratification, and recurrent pattern differentiation. Our results reveal the potential role of SGZ in recurrence aside from SVZ.

Introduction

Brain glioblastoma multiforme (GBM) is one of the most aggressive types of primary cancer, with a recurrence rate as high as 90% and a dismal 5-year survival of 4% to 5%.[1,2] The standard of care for patients with newly diagnosed GBM consists of maximal safe resection, followed by adjuvant therapies, among which external beam radiation therapy (RT) has long played a crucial role with demonstrated survival benefit over other supportive care.[3,4] Despite significant developments in image guided RT leading to improved definitive and salvage treatments, minimal improvement in GBM survival has been brought by RT since the introduction of temozolomide coadministration a decade ago. Recently, the development of tumor-treating fields has shown positive clinical trial results for further survival extension but debates are ongoing on its lack of mechanism of action, and no superior efficacy has been observed in the treatment of recurrent GBM.[5] Overall, the therapeutic outcomes in recurrence reduction continue to be disappointing.[6-8] The limited clinical success in GBM treatment highlights the inadequate understanding of tumorigenesis; thus, increasing tumor tissue profiling has been conducted at the genomic and proteomic level for the underpinning biology and better patient stratification.[8] However, although pathologic subtyping dictates tumor aggressiveness and the associated survival risks, it yields limited insights on the geometric location for more targeted RT planning.

Recently, increasing evidence has linked GBM pathogenesis with the involvement of stem cell niches (SCNs; ie, regions identifiable through radiographic images), providing new directions for RT treatment.[9-11] There are 2 main SCNs in the adult human brain: the larger subventricular zone (SVZ), which lines the wall of the lateral ventricles, and the smaller subgranular zone (SGZ), which resides in the hippocampus.[12,13] Isolated neural stem cells from these 2 regions are found to have shared cellular pathways with brain tumor cells and exhibit some glioma-like characteristics, such as angiogenesis association, immature antigenic phenotype possession, and, more importantly, a greater ability to migrate.[14-16] The role of SCN in GBM formation and progression has been further assessed through in vivo imaging analysis, in which a worse prognosis and more aggressive cancer spread have been associated with anatomic proximity to SCN.[17-19]

Additional evidence points to the positive correlation between incidental SCN dose from RT and patient survival.[4,20,21] However, the modest correlation is weakened by uncertainties from the heterogeneous geometric definition.[22] The radiologic definition of SCN is inconsistent among studies, with variations such as ipsilateral versus bilateral SVZ, various margins to ventricles, and with or without the inclusion of SGZ. As a result, SCN involvement could only be semi-quantitatively assessed (anatomic contact vs noncontact, distance to the wall of lateral ventricles). Given the proximity of SCN to several critical brain regions, such as the corpus callosum and hippocampus, further debates arose on increased toxicity over limited survival benefit. To date, there has been no consensus on a single SCN-based measurement for patient stratification and the optimized target dose and volume for SCN inclusion. Therefore, we need a novel quantitative SCN proximity assessment that is capable of achieving significantly more robust prediction for patient recurrence and survival analyses.

In the present study, we aimed to quantify the extent of SCN involvement for improved patient stratification and RT planning. On brain magnetic resonance imaging (MRI), we characterized the tumor proximity to SCN through the summed inverse distance to SCN, which captures a comprehensive spatial relationship between the tumor and all SCN zones (SVZ and SGZ). We then evaluated the effectiveness of these novel metrics as patient survival and recurrence location predictors.

Methods and Materials

Patient and imaging data

Two MRI data sets of patients with GBM were included in the study: preoperative scans of 237 patients, age 18 to 86 years (60.3 ± 12.8 years) from the Cancer Imaging Archive (used for prognostic stratification),[23,24] and follow-up scans of 55 patients, age 18 to 74 years (51.1 ± 13.9 years), retrospectively solicited from our institutional database (used for recurrence pattern identification). The preoperative data set consists of multicenter, multivendor MRI scans with field strengths of 1.5T or 3T and slice thickness of 1 to 6 mm. Four sequences were included for each patient: T1-weighted (T1), T1 contrast-enhanced (T1ce), T2-weighted (T2), and T2 fluid-attenuated inversion recovery (FLAIR). The delineation of the tumor volumes (enhancing and nonenhancing tumor regions) was provided with the data sets and assessed by a radiologist.[24] The patients with GBM from the follow-up data set were retrospectively solicited from our institutional databases according to the following criteria: (1) had surgical resection; (2) had clinically diagnosed recurrence; and (3) received MRI scans at the time of recurrence. MRI images of the same 4 sequences were obtained on 3 scanners: GE Signa Excite 1.5T and 3T scanners, as well as SIEMENS Avanto 1.5T scanner. Slice

thickness ranged from 2 to 5 mm. Primary tumor volumes (we used resection cavities in this study) and recurrence volumes were manually segmented, mainly on T1ce images, with other sequences for complementary assessments.

Stem cell niche delineation and generation of proximity map

Four SCN zones were defined in the T1-MR Montreal Neurological Institute (MNI) brain template, as shown in Figure 1.[25] Specifically, bilateral SVZs were defined as the 3 to 5 mm extension outside the wall of each lateral ventricle, and bilateral SGZs were defined at the interface between the hilus and the granular layer of each hippocampus.[12,13] As a common representation in most neurogenic niche-related research, lateral ventricles (LVs) were also delineated for each patient to facilitate traditional distance-to-ventricle measurements for comparison purposes. The delineation of LVs was initiated by registration-based warping from a template and followed by manual editing.[25]

To quantitatively characterize the degree of tumor−SCN proximity, a normalized proximity map was generated using the inverse distance (ID) weightings to voxel-wise observations in the corresponding SCN. Specifically, the proximity to SVZ, the largest and most commonly referred SCN, is estimated as

$$PS_{SVZ}(x) = \begin{cases} \dfrac{ID(x) - ID_{\min}}{ID_{\max} - ID_{\min}}, if\ x \notin V \\ 1, if\ x \in V \end{cases} \quad (1)$$

where

$$ID(x) = \sum_{i=1}^{N} \frac{1}{d(x,\ V_i)^2} \quad (2)$$

$V_i\ with\ i \in [1, N]$ represents an observation in bilateral SVZ, and x is an interpolated voxel in the brain. $d(x,\ V_i)^2$denotes the squared Euclidean distance between x and a given observation in V. ID_{max} and ID_{min} correspond to the maximum and minimum inversed distance within V, respectively.

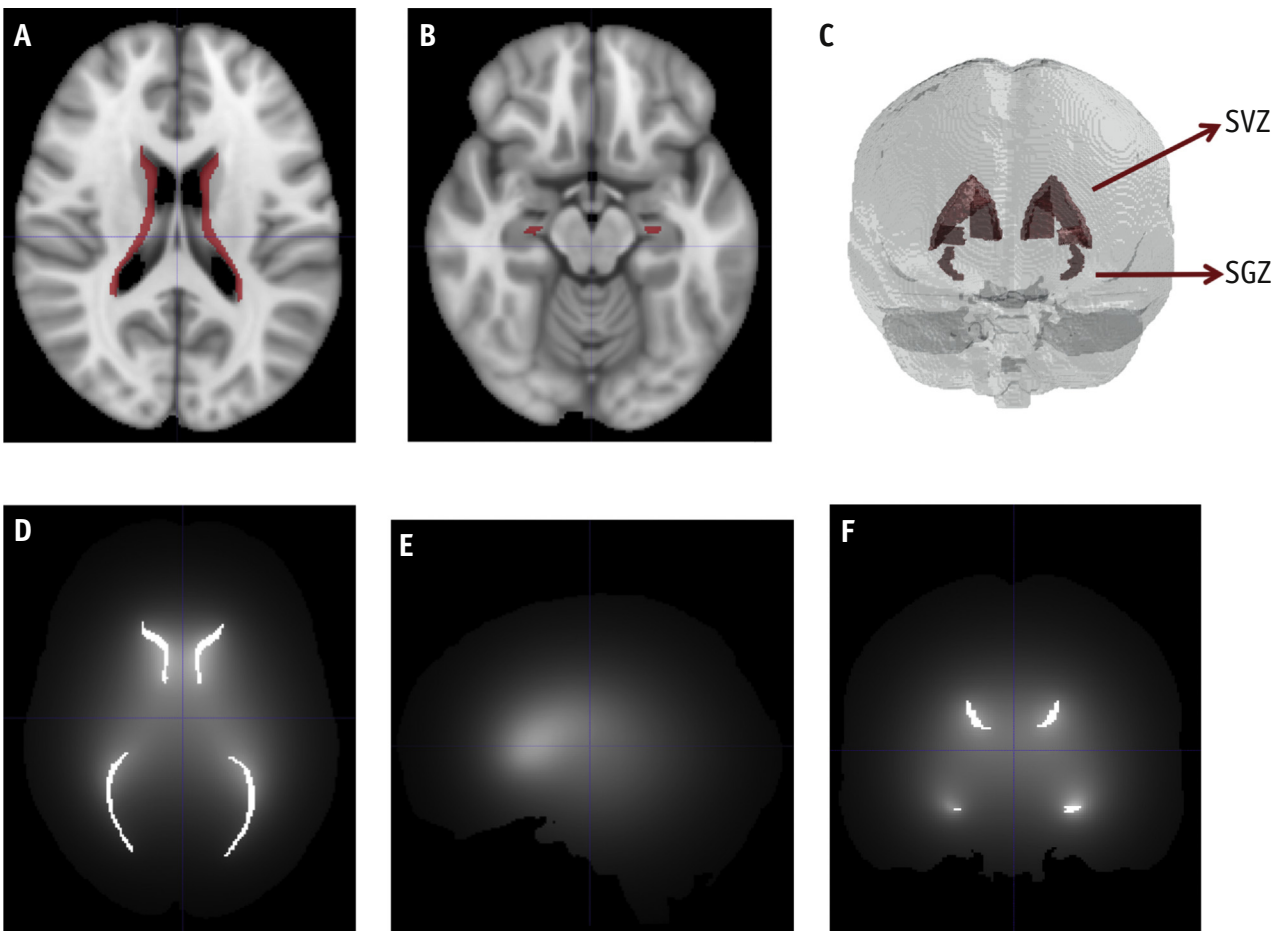

Fig. 1. Two brainstem cell zones, showing the (A) subventricular zone, and (B) subgranular zone, as well as a (C) 3-dimensional rendering of segmented bilateral subventricular and subgranular zones, and (D) axial, (E) sagittal, and (F) coronal views of the proximity map with intensities illustrating the degree of proximity to all stem cell niches. All images are visualized in ITK-SNAP (www.itksnap.org).

Similarly, PS_{SGZ} is calculated for the less explored SGZ. Accounting for the impact of all SCN zones, PS_{SCN} is finally calculated as the sum of PS_{SVZ} and PS_{SGZ}, normalized between 0 and 1. All proximity calculations were conducted using in-house codes built in MATLAB (version 9.6.0.1072779 [R2019a]; The MathWorks Inc., Natick, MA). A visual illustration of the resulting PS_{SCN} map is shown in Figure 1.

Image processing

To remove individual variances of brain size and shape on proximity measurements, we preprocessed each T1 MRI by stripping the skull, conducting bias field correction, and performing affine registration to the common template space using SimpleITK and FSL.[26,27] Subsequently, pathology adaptive deformable registration was performed on each of the patients to afford finer tissue alignment with the template, using state-of-the-art symmetrical normalization diffeomorphic registration in advanced neuroimaging tools.[25,28] Specifically, the MNI template was deformably aligned to each patient, with similarity enforcement applied only in the nonpathologic tissues, excluding the non-corresponding lesioned areas (ie, tumor or cavities). Next, the inverse transformations were propagated onto the tumor and the LV segmentation.

The mean and maximum proximity scores (PS) to the SVZ (PS_{m-SVZ} and $PS_{max-SVZ}$) and all SCNs (PS_{m-SCN} and $PS_{max-SCN}$) were calculated for each primary/recurrent tumor volume, deformably transformed into the common template space. In addition, 2 traditional SCN-related proximity metrics, tumor edge to the ventricle (EV) and center to the ventricle (CV), were included for comparison. EV and CV measurements were calculated as the minimal distances between the edge or center of the tumor cores to the wall of the lateral ventricles, using brutal force point-to-point distance calculations between 2 binarized structures. Owing to the sensitivity of these point measurements to individual patient anatomy, to maximally preserve the morphology, the EV and CV calculations were performed in the subject space with only affine alignment to the common template.

Statistical Analysis

The prognostic values of the 4 PS-based metrics (PS_{m-SVZ}, $PS_{max-SVZ}$, PS_{m-SCN}, and $PS_{max-SCN}$) were first evaluated using univariate Cox proportional hazards regression with overall survival (OS). OS was defined as the period from the time of diagnosis to the time of patient death or last encounter. Given the wide range of patient age in the data set (range, 18-86 years) and the confounding role of age,[29,30] multivariate Cox regression was also performed for each predictor to account for the age effect. To assess the classification capacity of each risk predictor, we stratified all patients into 2 risk groups based on 2 methods: M1, sorted and evenly divided high-risk (HG) and low-risk (LG) groups; and M2, automatically clustered HG and LG using K-means with the city block distance. For comparison, we performed the same analyses on traditional EV and CV measurements.

To further evaluate the impact of SCNs on recurrence patterns, group comparisons were performed between the primary and recurrent tumors in terms of 4 PS-derived metrics and the 2 traditional measurements for comparison. All statistical analyses were performed in MATLAB (version 9.6.0.1072779 [R2019a]; The MathWorks Inc; Natick, MA).

Results

Preoperative prognostic capacity

Table 1 shows the Cox regression results of all predictors. Among all tested metrics, the PS_{SCN}-derived metrics were the best OS predictors, with or without adjusting for age. In particular, PS_{m-SCN} (ie, degree of overall tumor core proximity to all SCN zones) significantly predicted OS ($P < .0001$) with a hazard ratio of 10.28 (95% confidence interval, 3.1841-33.2289), indicating a drastically increased

Table 1 Results of Cox proportional hazards regression between overall survival and 6 stem cell region-associated predictors (CV, EV, PS_{m-SVZ}, $PS_{max-SVZ}$, PS_{m-SCN}, $PS_{max-SCN}$), as well as age

	Mean	Standard deviation	Hazard ratio	95% confidence interval	*P*-value
Age, y	60.35	12.84	1.03	1.02-1.05	5.5034e-10*
CV, mm	19.40	15.11	0.99	0.99-1.00	.7870
			0.99	0.98-1.00	.3239
EV, mm	5.39	7.92	0.98	0.96-1.00	.0601
			0.98	0.96-0.99	.0399†
PS_{m_SVZ}	0.26	0.11	2.58	0.86-7.74	.0890
			5.02	1.64-15.35	.0046*
PS_{max_SVZ}	0.71	0.30	1.76	1.12-2.76	.0137†
			1.77	1.13-2.77	.0116†
PS_{m_SCN}	0.26	0.11	5.17	1.66-16.07	.0045*
			10.28	3.18-33.22	9.7867e-05*
PS_{max_SCN}	0.75	0.30	2.06	1.30-3.27	.0019*
			2.05	1.29-3.24	.0021*

Abbreviations: CV = tumor center to the ventricle; EV = tumor edge to the ventricle; PS_{m-SVZ} = mean proximity score of the subventricular zone, $PS_{max-SVZ}$ = maximum proximity score of the maximum subventricular zone; PS_{m-SCN} = mean proximity score of the stem cell niche; $PS_{max-SCN}$ = maximum proximity score of the stem cell niche.

Results of univariate Cox regression are shown in light gray colored rows, and the ones adjusted for age are shown in dark gray.

* *P*-values <.01.

† *P*-values <.05.

Table 2 Results of log-rank tests for patient risk groups stratified by 6 imaging-based metrics, using M1 and M2

	Low-risk group			High-risk group					
	n	Mean	SD	n	Mean	SD	Hazard ratio	95% confidence interval	*P*-value
CV	118	32.25	9.72	119	6.66	5.86	0.89	0.67-1.17	.4534
	119	32.13	9.78	118	6.57	5.80	0.87	0.66-1.15	.3975
EV	118	9.84	9.32	119	0.99	0.05	0.93	0.71-1.23	.7072
	51	19.02	6.67	186	1.66	1.66	0.81	0.59-1.09	.2042
PS_{m_SVZ}	119	0.17	0.03	118	0.35	0.10	0.71	0.54-0.94	.0205*
	162	0.19	0.04	75	0.40	0.09	0.77	0.57-1.05	.1205
PS_{max_SVZ}	119	0.43	0.17	118	1.00	0.00	0.70	0.53-0.93	.0178*
	113	0.40	0.12	124	0.99	0.01	0.68	0.51-0.90	.0091†
PS_{m_SCN}	119	0.17	0.03	118	0.35	0.09	0.62	0.47-0.83	.0015†
	138	0.18	0.04	99	0.37	0.08	0.70	0.53-0.94	.0227*
PS_{max_SCN}	119	0.50	0.24	118	1.00	0.00	0.56	0.42-0.75	.0001†
	99	0.40	0.12	140	0.99	0.04	0.66	0.50-0.87	.0045†

Abbreviations: CV = tumor center to the ventricle; EV = tumor edge to the ventricle; PS_{m-SVZ} = mean proximity score of the subventricular zone, $PS_{max-SVZ}$ = maximum proximity score of the maximum subventricular zone; PS_{m-SCN} = mean proximity score of the stem cell niche; $PS_{max-SCN}$ = maximum proximity score of the stem cell niche; SD = standard deviation

Log-rank statistics of groups stratified using M1 and M2 are displayed in light and dark gray rows, respectively.

* *P*-values <.05.

† *P*-values <.01.

survival risk with closer SCN proximities. The next best OS predictor is $PS_{max-SCN}$ (ie, extent of the closest vicinity of the tumor core to all SCN zones; univariate $P = .0019$; age-adjusted $P = .0021$). Proximity estimation based on SVZs only, $PS_{max-SVZ}$ and PS_{m-SVZ}, also presented associations with OS, but to a lesser degree of significance. The 2 traditional distance-based metrics (CV and EV) are ineffective in predicting OS, with highly varying HR values that fluctuated around 1.

The risk stratification capability of each metric was further validated using the log-rank test, as shown in Table 2. Kaplan-Meier survival curves of groups stratified using M1 and M2 can be found in Figure 2A and 2B, respectively. The survival risks were best stratified by $PS_{max-SCN}$, using both evenly divided and K-means clustering methods, with *P*-values of .0001 and .0045, respectively. Consistently, in both methods, PS metrics derived from all SCN zones outperformed those derived from SVZ alone. Again, the traditional CV and EV metrics were unable to stratify the risks using even division or K-means clustering.

Recurrence pattern differentiation

As shown in Figure 3, the difference in anatomic distributions between primary and recurrent tumors is reflected in the composite map of tumors from all patients. A 3-dimensional rendering of accumulated primary versus recurrent tumors (shown in red and green, respectively) revealed more medial/central located recurrence. In other words, recurrent tumors showed a decreased distance to the ventricles and increased proximities to SCNs. The medial/central shift between primary and recurrent tumors was successfully detected by 3 tumor center-/average-related metrics: PS_{m-SCN}, PS_{m-SVZ}, and CV, with *P*-values of .0225, .0321, and .0243, respectively. The remaining 3 edge/maximal PS-related metrics ($PS_{max-SCN}$, $PS_{max-SVZ}$, and EV) failed to detect the collective shift. More detailed statistical results of the primary and recurrence comparisons can be found in Table 3.

Discussion

The connection of adult brain SCN with glioma pathogenesis dates back 2 decades ago when accumulating cancerogenesis evidence suggested that gliomas arose from transformed endogenous stem cells rather than fully differentiated glia, as was long believed.[9,14] As imaging techniques advanced, the in vivo association between GBM and SCNs have been reappraised in patients. The majority of these studies focused on SVZ, the largest SCN in the adult brain. In particular, Jafri et al classified 91 patients with GBM according to their primary tumor location in relation to the SVZ and cortex and found decreased OS and progression-free survival in SVZ-contacting group, regardless of cortical involvement.[17] However, using similarly classified groups according to SVZ abutment on 49 patients, Kimura et al found no relation between GBM location with respect to SVZ and recurrence patterns (local, spread, distant).[31] Subsequently, Adeberg et al further evaluated 607 patients with GBM and confirmed the association of SVZ involvement with shorter survival and distant progression.[18] Different from the coarse binary grouping method based on SVZ contact, Liu et al refined the definition of SVZ involvement using the shortest distances from the tumor centroid to the edge of the lateral ventricles and reported poorer prognosis in patients with

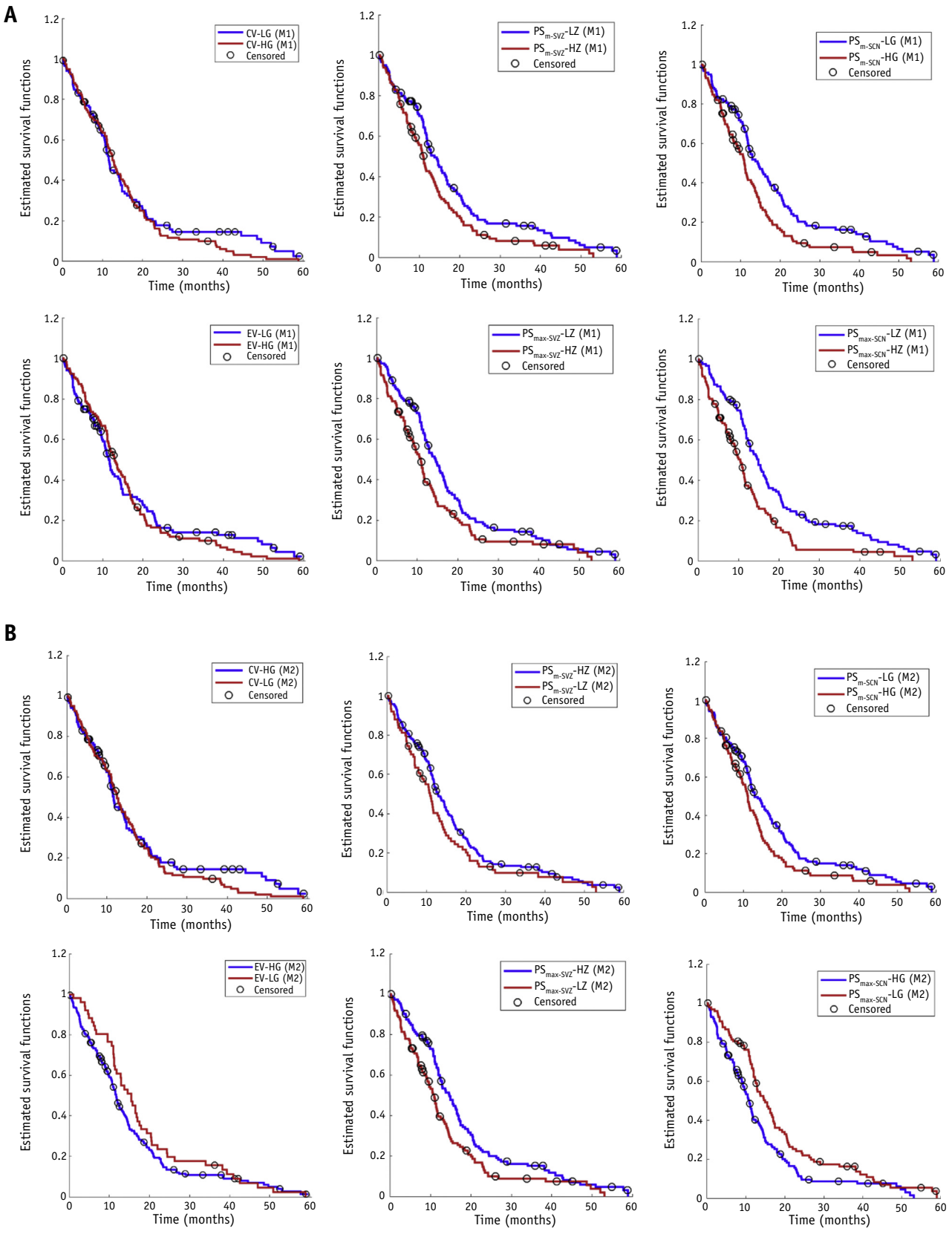

Fig. 2. Kaplan-Meier plots of overall survival for groups of patients stratified by 6 stem cell niche-associated metrics, using (A) evenly dividing method (M1, and (B) K-means clustering (M2). Censored observations are marked by black circles.[37] (A color version of this figure is available at https://doi.org/10.1016/j.ijrobp.2021.02.020.)

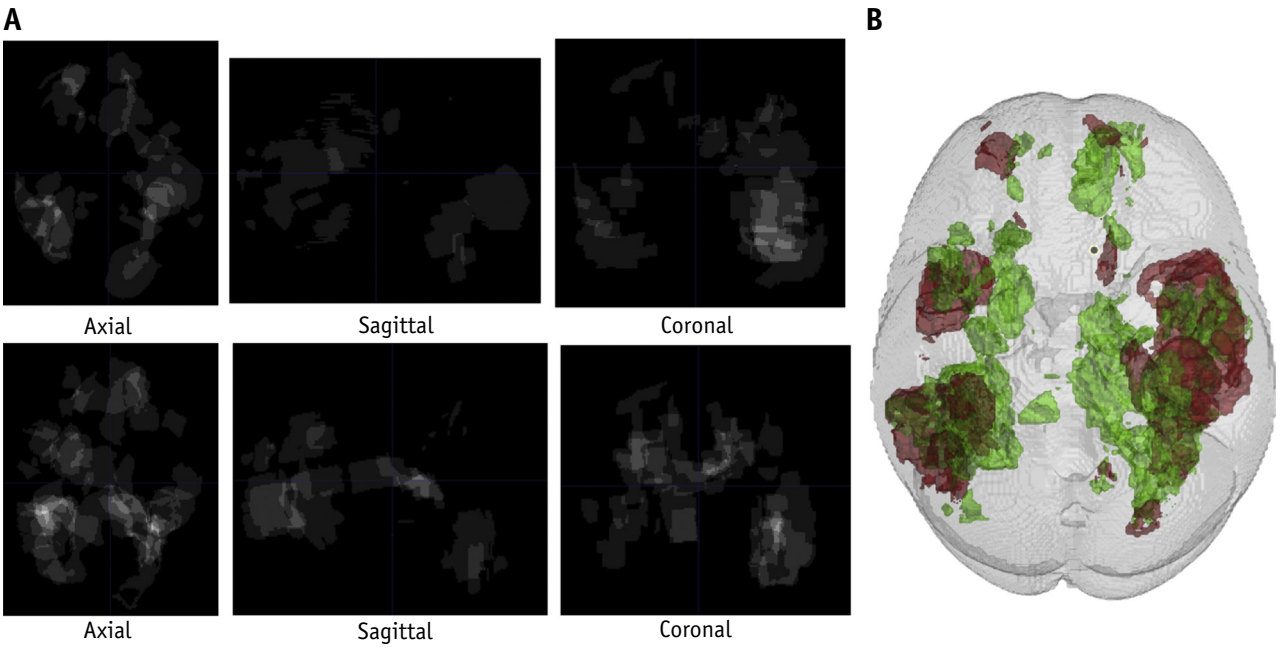

Fig. 3. Overlaid primary and recurrent tumor locations from all subjects, showing (A) axial, sagittal, and coronal views for primary (upper row) and recurrent (bottom row) tumors, and (B) 3-dimensional rendering of primary (red) and recurrent (green) tumors. Primary and recurrent tumors show significant differences in proximity to stem cell niches (medial and center located), using 3 centroid/mean proximity score-based metrics. (A color version of this figure is available at https://doi.org/10.1016/j.ijrobp.2021.02.020.)

low-grade glioma with shorter distances to the ventricles.[19] However, as shown by our study, the point−distance metrics for classification suffer from high variance and are unreliable predictors of OS and risks.

Previous SCN-derived GBM studies focused on SVZ, but the prognostic role of SGZ, the relatively smaller neurogenic niche in the adult brain, has been inadequately explored. Located between the granule cell layer and hilus of the dentate gyrus of the hippocampus, the SGZ is concomitantly spared in advanced hippocampal-sparing RT plans aiming for maximal memory preservation.[32,33] As a result, evidence supporting the contribution of SGZ in GBM formation and recurrence may increase the need for a more comprehensive evaluation of neurocognitive function protection over compromised target coverage. However, in the few studies that incorporated the SGZ into survival and recurrence analysis, split findings were reported. For instance, among 102 patients with GBM, Chen et al defined neurogenic region (NR) involvement as the direct contact of the contrast-enhancing tumor edge with either SVZ and SGZ and revealed a qualitative propensity of GBM to recur toward NRs.[34] In contrast, Mistry et al compared survival between groups with or without contact with each NR. Among 207 patients with GBM, they found that the adverse prognostic effect is specific to SVZ contact, but the SGZ contact group was small in their data set (10% of the entire cohort).[35]

To improve the quantification of the geometric correlation and better elucidate the role of SGZ in GBM outcome and recurrence, we developed an inverse distance-based proximity estimation on structural MRI in the current study to quantify the extent of SCN involvement in GBM. Using the cumulative inverse distances for both SVZ and SGZ, the contributions of both neurogenic niches are combined into a single proximity map, where the influence of SCN on the tumor, gauged by the location of the tumor on the map, can be effectively characterized. Among 237 patients with GBM from the public Cancer Imaging Archive data set, the inverse distance-derived metrics outperformed traditional

Table 3 Group comparison results between primary and recurrent tumors using 6 stem cell niche-derived metrics

	Primary		Recurrence		
	Mean	SD	Mean	SD	*P*-value
CV, mm	21.00	11.71	18.64	10.85	.0243*
EV, mm	6.75	7.93	6.75	7.79	.9974
PS_{m_SVZ}	0.23	0.13	0.26	0.12	.0225*
PS_{max_SVZ}	0.65	0.33	0.66	0.32	.8308
PS_{m_SCN}	0.22	0.12	0.24	0.11	.0321*
PS_{max_SCN}	0.68	0.32	0.66	0.32	.5175

Abbreviations: CV = tumor center to the ventricle; EV = tumor edge to the ventricle; PS_{m-SVZ} = mean proximity score of the subventricular zone; $PS_{max-SVZ}$ = maximum proximity score of the maximum subventricular zone; PS_{m-SCN} = mean proximity score of the stem cell niche; $PS_{max-SCN}$ = maximum proximity score of the stem cell niche; SD = standard deviation.

* *P*-values <.05.

edge or center distance-based measurements in preoperative OS prediction and survival risk stratification. PS based on the SVZ alone (PS_{m-SVZ} and $PS_{max-SVZ}$) reached moderate significance in the aforementioned prognostic testing, but a collective proximity estimation combining the SVZ and SGZ estimation (PS_{m-SCN} and $PS_{max-SCN}$) evidently improved the prognostic power. Moreover, the tendency of GBM to recur closer to SCN was confirmed by 3 centroid-/average-based measurements, specifically as significantly higher PS_{m-SVZ} and PS_{m-SCN}, as well as significantly shorter CV. The systematic shift between primary and recurrent tumors further implicates the role of SCNs in GBM progression. For RT, our results provide more robust evidence for personalized RT to offset the potential toxicity associated with the high-risk volumes.

Our study is not without remaining questions. First, the manually defined SCN on the common MNI space and the use of generic-lesion-purposed registration. The MNI template created on healthy adults may not fully represent the anatomy of pathologic GBM brains with, for instance, enlarged ventricles and degenerated white matter. The difference may introduce errors in brain registration and manual identification of SCN, especially those contacting the lateral ventricles. In addition, the lesion-based advanced neuroimaging tool registration, although being the current state-of-the-art method for pathologic brain alignment, may not fully account for specific morphologic characteristics (relatively large deformations around the ventricles and cavities) for GBM brains. A separate investigation beyond the scope of the current study, such as a brain template specific to the GBM population and an algorithm adaptive to pathologic GBM brains,[36] would be needed to focus on the accuracy of brain alignment and SCN delineation.

Second, our analyses were only controlled for age. The prognostic power of PS-derived metrics, especially those obtained on all SCN zones, are consistent with and without age adjustment. Nevertheless, other confounding factors, such as the O6-methylguanine-DNA methyltransferase promoter methylation status, preoperative Karnofsky performance status score, treatment regimens, and resection status, may exist and require further analysis. Third, although 3 metrics concomitantly identified a closer distribution of recurrence to SCN, including SGZ, into the analyses, they did not improve the power of group differentiation. Whether this is specific to our limited number of patients in the recurrence data set or due to a more complex mechanism of recurrence (ie, collective contribution of primary tumor infiltration and SCN) is unclear. A substantially larger data set may be needed to shed light on these questions.

Conclusions

We introduced a novel inverse distance-based metric to comprehensively characterize the anatomic proximity of GBM tumors to SCN zones. The PS derived from all SCN zones outperformed those derived from SVZ alone, as well as traditional edge or center distance-based measurements in OS prediction and risk stratification. Our results implicate the potential role of SGZ in recurrence aside from SVZ. Moreover, both traditional and inverse distance-based metrics concomitantly detect a central-shift pattern of recurrence, further implying the role of SCN in GBM recurrence.

References

1. Stupp R, Hegi ME, Mason WP, et al. Effects of radiotherapy with concomitant and adjuvant temozolomide versus radiotherapy alone on survival in glioblastoma in a randomised phase III study: 5-year analysis of the eortc-ncic trial. *Lancet Oncol* 2009;10:459-466.
2. van Linde ME, Brahm CG, de Witt Hamer PC, et al. Treatment outcome of patients with recurrent glioblastoma multiforme: A retrospective multi-center analysis. *J Neurooncol* 2017;135:183-192.
3. Walker MD, Green SB, Byar DP, et al. Randomized comparisons of radiotherapy and nitrosoureas for the treatment of malignant glioma after surgery. *N Engl J Med* 1980;303:1323-1329.
4. Batash R, Asna N, Schaffer P, Francis N, Schaffer M. Glioblastoma multiforme, diagnosis and treatment; recent literature review. *Curr Med Chem* 2017;24:3002-3009.
5. Mehta M, Wen P, Nishikawa R, Reardon D, Peters K. Critical review of the addition of tumor treating fields (TTFields) to the existing standard of care for newly diagnosed glioblastoma patients. *Crit Rev Oncol Hematol* 2017;111:60-65.
6. Mann J, Ramakrishna R, Magge R, Wernicke AG. Advances in radiotherapy for glioblastoma. *Front Neurol* 2018;8:748.
7. Kazda T, Dziacky A, Burkon P, et al. Radiotherapy of glioblastoma 15 years after the landmark Stupp's trial: More controversies than standards? *Radiol Oncol* 2018;52:121-128.
8. Taylor OG, Brzozowski JS, Skelding KA. Glioblastoma multiforme: An overview of emerging therapeutic targets. *Front Oncol* 2019;9:963.
9. Sanai N, Alvarez-Buylla A, Berger MS. Neural stem cells and the origin of gliomas. *N Engl J Med* 2005;353:811-822.
10. Alcantara Llaguno S, Chen J, Kwon CH, et al. Malignant astrocytomas originate from neural stem/progenitor cells in a somatic tumor suppressor mouse model. *Cancer Cell* 2009;15:45-56.
11. Altmann C, Keller S, Schmidt MHH. The role of SVZ stem cells in glioblastoma. *Cancers (Basel)* 2019;11:448.
12. Sanai N, Tramontin AD, Quinones-Hinojosa A, et al. Unique astrocyte ribbon in adult human brain contains neural stem cells but lacks chain migration. *Nature* 2004;427:740-744.
13. Eriksson PS, Perfilieva E, Björk-Eriksson T, et al. Neurogenesis in the adult human hippocampus. *Nat Med* 1998;4:1313-1317.
14. Reya T, Morrison SJ, Clarke MF, Weissman IL. Stem cells, cancer, and cancer stem cells. *Nature* 2001;414:105-111.
15. Tomasetti C, Li L, Vogelstein B. Stem cell divisions, somatic mutations, cancer etiology, and cancer prevention. *Science* 2017;355:1330-1334.
16. Lee JH, Lee JE, Kahng JY, et al. Human glioblastoma arises from subventricular zone cells with low-level driver mutations. *Nature* 2018;560:243-247.
17. Jafri NF, Clarke JL, Weinberg V, Barani IJ, Cha S. Relationship of glioblastoma multiforme to the subventricular zone is associated with survival. *Neurooncol* 2013;15:91-96.
18. Adeberg S, König L, Bostel T, et al. Glioblastoma recurrence patterns after radiation therapy with regard to the subventricular zone. *Int J Radiat Oncol Biol Phys* 2014;90:886-893.
19. Liu S, Wang Y, Fan X, et al. Anatomical involvement of the subventricular zone predicts poor survival outcome in low-grade astrocytomas. *PloS One* 2016;11:e0154539.

20. Khalifa J, Tensaouti F, Lusque A, et al. Subventricular zones: New key targets for glioblastoma treatment. *Radiat Oncol* 2017;12:67.
21. Lee P, Eppinga W, Lagerwaard F, et al. Evaluation of high ipsilateral subventricular zone radiation therapy dose in glioblastoma: A pooled analysis. *Int J Radiat Oncol Biol Phys* 2013;86:609-615.
22. Sharma A, Munshi A, Mohanti BK. Evaluation of high ipsilateral subventricular zone radiation therapy dose in glioblastoma: A pooled analysis. In regard to Lee et al. *Int J Radiat Oncol Biol Phys* 2013;87:631.
23. Clark K, Vendt B, Smith K, et al. The Cancer Imaging Archive (TCIA): Maintaining and operating a public information repository. *J Digit Imaging* 2013;26:1045-1057.
24. Bakas S, Akbari H, Sotiras A, et al. Advancing the cancer genome atlas glioma MRI collections with expert segmentation labels and radiomic features. *Sci Data* 2017;4:170117.
25. Grabner G, Janke AL, Budge MM, Smith D, Pruessner J, Collins DL. Symmetric atlasing and model-based segmentation: An application to the hippocampus in older adults. *Med Image Comput Comput Assist Interv* 2006;9:58-66.
26. Tustison NJ, Avants BB, Cook PA, et al. N4ITK: Improved N3 bias correction. *IEEE Transact Med Imaging* 2010;29:1310-1320.
27. Jenkinson M, Beckmann CF, Behrens TEJ, Woolrich MW, Smith SM. FSL. *Neuroimage* 2012;62:782-790.
28. Avants BB, Tustison NJ, Song G, Cook PA, Klein A, Gee JC. A reproducible evaluation of ants similarity metric performance in brain image registration. *Neuroimage* 2011;54:2033-2044.
29. Walid MS. Prognostic factors for long-term survival after glioblastoma. *Perm J* 2008;12:45.
30. Smrdel U, Skoblar Vidmar M, Smrdel A. Glioblastoma in patients over 70 years of age. *Radiol Oncol* 2018;52:167-172.
31. Kimura M, Lee Y, Miller R, Castillo M. Glioblastoma multiforme: Relationship to subventricular zone and recurrence. *Neuroradiol J* 2013;26:542-547.
32. Gondi V, Pugh SL, Tome WA, et al. Preservation of memory with conformal avoidance of the hippocampal neural stem-cell compartment during whole-brain radiotherapy for brain metastases (RTOG 0933): A phase II multi-institutional trial. *J Clin Oncol* 2014;32:3 810.
33. Hofmaier J, Kantz S, Söhn M, et al. Hippocampal sparing radiotherapy for glioblastoma patients: A planning study using volumetric modulated arc therapy. *Radiat Oncol* 2016;11: 118.
34. Chen L, Chaichana KL, Kleinberg L, Ye X, Quinones-Hinojosa A, Redmond K. Glioblastoma recurrence patterns near neural stem cell regions. *Radiother Oncol* 2015;116:294-300.
35. Mistry AM, Dewan MC, White-Dzuro GA, et al. Decreased survival in glioblastomas is specific to contact with the ventricular-subventricular zone, not subgranular zone or corpus callosum. *J Neurooncol* 2017; 132:341-349.
36. Lao Y, Yu V, Chang E, Yang W, Sheng K. Deformable alignment of longitudinal postoperative brain GBM scans using deep learning. *Med Imaging* 2020;11313:113130.
37. Curve Cardillo G. KMPLOT: Kaplan−Meier estimation of the survival function. Available at: http://www.mathworks.com/matlabcentral/fileexchange/22293. Accessed July 1, 2020.